J. Phys. B: At. Mol. Opt. Phys. **41** (2008) 185202 (10pp) doi:10.1088/0953-4075/41/18/185202

Cross sections for elastic electron collisions on two hydrocarbon compounds: *n*-butane and benzene in the intermediate-energy range

I P Sanches[1], R T Sugohara[2], L Rosani[1], M-T Lee[1] and I Iga[1]

[1] Departamento de Química, UFSCar, 13565-905 São Carlos, SP, Brazil
[2] Departamento de Física, UFSCar, 13565-905 São Carlos, SP, Brazil

Received 21 April 2008, in final form 20 June 2008
Published 3 September 2008
Online at stacks.iop.org/JPhysB/41/185202

Abstract
In this work, we report an experimental-cross-section determination of elastic electron collisions with two hydrocarbon species, namely *n*-butane and benzene, in the intermediate-energy range. More specifically, absolute differential, integral and momentum-transfer cross sections are measured and reported in the (50–1000) eV range. The measurements were performed using a crossed electron beam–molecular beam geometry. The angular distributions of the scattered electrons were converted to absolute cross sections using the relative flow technique. Integral and momentum-transfer cross sections are derived from the measured differential cross sections. Additionally, elastic cross sections are also calculated using the independent atom model at the static-exchange-polarization level of approximation. A comparison of our measured data with calculated and other experimental results available in the literature is made.

1. Introduction

Electron collisions with small polyatomic hydrocarbon molecules is a subject of increasing interest, both theoretically and experimentally, due to the role played by these compounds in various fields of application [1, 2]. For instance, hydrocarbon plasmas are often present in industrial reactors, in the ignition and combustion of fuels, in the interstellar medium as well as in some planetary atmospheres. Particularly, in plasma-assisted combustion researches [3, 4], the large and stable fuel molecules are cracked by electron-impact dissociation processes. Smaller fragments including stable molecules and free radicals are generated. Such radicals are short-lived and highly reactive species which make the combustion faster, cleaner and more complete. Quantitative cross section data may be useful to understand conditions of such nonthermal plasmas. In this regard, there is a general interest on studies of electron interaction with hydrocarbon compounds. Specifically *n*-butane has many applications. It is well known that the liquified petroleum gas, an important alternative fuel for automobiles, is a mixture of propane and butane of almost equal proportions. At room temperature and normal atmospheric pressure conditions, C_4H_{10} is a gas. However, it liquefies at moderately higher pressures and afterwards, it vaporizes rapidly upon release of pressure. Such properties allow easy transportation and storage of this compound in the liquid phase. In this consequence, extensive applications are found for butanes such as fuel, propellant for aerosols, lighting, to cite just a few. It is also being considered for use as refrigerants as an alternative to chlorofluorocarbons, which are known to cause deterioration of the Earth's ozone layer. In addition, *n*-butane is also contained in commercial gasolines, with research grade octane number of 94 [5].

Like butane, benzene is also a very important chemical compound. It is a key precursor in many chemical synthesis used in pharmaceutical and petrochemical industries. Besides, it plays an important role in the chemistry of planetary atmospheres. For instance, it takes part on the mechanism of haze formation in Titan's atmosphere [6]. Also, it has been observed in the C-rich protoplanetary nebula CRL618 [7],

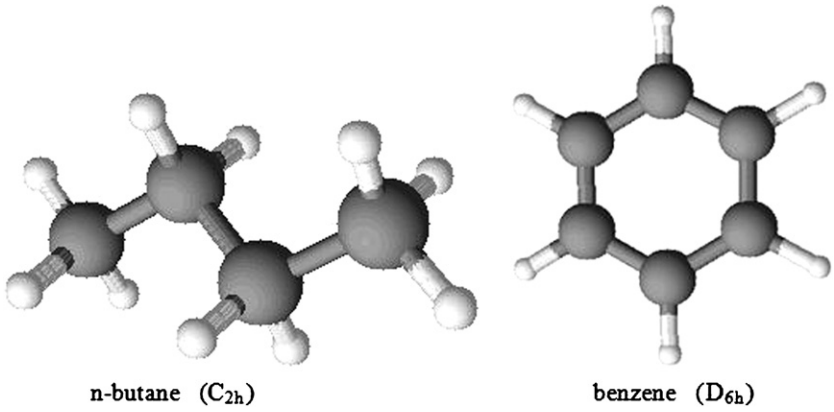

Figure 1. Molecular structures of *n*-butane and benzene. Dark spheres, carbon atoms; small white spheres, hydrogen atoms.

which represents the first detection of an aromatic compound out of the solar system.

From the theoretical point of view, the study of electron collisions on *n*-butane and benzene is also interesting because they represent models for the creation of theoretical methods for larger hydrocarbon systems, a field under current development [8–12].

Despite that, only very few experimental cross sections were reported for *n*-butane and benzene in the literature [13]. Some experimental grand-total cross sections (TCS) for *n*-butane were reported [14, 15]. Electron-impact partial (PICS) and total (TICS) ionization cross sections for *n*-butane were reported by Jiao *et al* [5] in the (10–200) eV energy range. Additionally, experimental TICS for *n*-butane were reported by Schram *et al* [16] in the (600–12000) eV energy range. Nevertheless, to our knowledge, there is no experimental measurement of differential (DCS), integral (ICS) and momentum-transfer (MTCS) cross sections for elastic electron scattering by this target in the literature.

For benzene, experimental results for electron collision cross sections are equally scarce. Some experimental grand-total cross sections (TCS) for electron–benzene scattering were reported [17–20] in a wide energy range. Electron-impact dissociative excitation cross sections for this target were measured by Beenakker and De Heer [21] in the (30–1000) eV energy range using a radiation emission technique. Schram *et al* [16] also reported experimental TICS for benzene in the (600–12000) eV energy range. A few experimental DCS for elastic electron–benzene scattering were reported by Gulley and Buckman [22] and Cho *et al* [23] at incident energies up to 40 eV. Very recently, DCS at very limited scattering angles were reported by Boechat-Roberty *et al* [24] at the incident energy of 1000 eV. Some relative DCS for elastic scattering by benzene at (300–900) eV energy range and 30°–120° angular range were reported by Mahant Shetty *et al* [25].

On the theoretical side, several investigations on elastic electron collisions with *n*-butane and benzene are reported in the literature. The calculation of cross sections for low-energy (10–50) eV electron scattering by *n*-butane was carried out by Lopes *et al* [12] using the Schwinger multichannel method (SMC) at the static-exchange (SE) level. More recently, Bettega *et al* [26] reported a theoretical study of elastic electron scattering by *n*-butane and its isomer (isobutane) in the (1–20) eV range also using the SMC, but at the static-exchange-polarization (SEP) level of approximation. Electron scattering by benzene at energies up to 40 eV was investigated by Gianturco and Lucchese [10] using the single-centre-expansion methods at the SE level of approximation and by Bettega *et al* [11], using SMC at both the SE and the SEP levels of approximation, limited to energies up to 30 eV. At intermediate and high energies, Ma *et al* [27] reported DCS, ICS and MTCS for *n*-butane and benzene in the 100–1000 eV range using the independent atom model (IAM). In their studies, a static-exchange-polarization interaction potential plus a modified absorption contribution (SEPA) is used to represent the electron–atom interaction dynamics and an extended structural factor is also applied in order to take partially account of the overlapping of electronic clouds between the adjacent atoms. Moreover, several theoretical calculations of TCS for electron scattering by benzene using different versions of additivity rule (AR) were also reported [28–31].

It is well known that at intermediate incident energies, ranging from the ionization threshold of the target to 1000 eV, the absorption effects are very important. In this energy range, most inelastic channels (electronic excitations, ionization, etc) are open, thus resulting in a reduction of the flux corresponding to the elastic channel. Recently, our group has conducted investigations on the influence of such effects in electron collisions with molecular targets in the intermediate energy range [32, 33]. For that, experimental DCS, ICS and MTCS in this range are required in order to test the validity of theoretical models.

In this work, we report an experimental investigation on elastic electron scattering by *n*-butane and benzene. Absolute DCS determined in the (50–1000) eV range using the relative flow technique (RFT) [34–36] are reported. ICS and MTCS in this range are also derived from the experimental DCS, measured in the 10°–130° angular range and extrapolated to forward and backward directions. Elastic DCS, ICS and MTCS are also calculated using the IAM at the SEP level of approximation. Figure 1 shows the chemical structures of these two molecules.

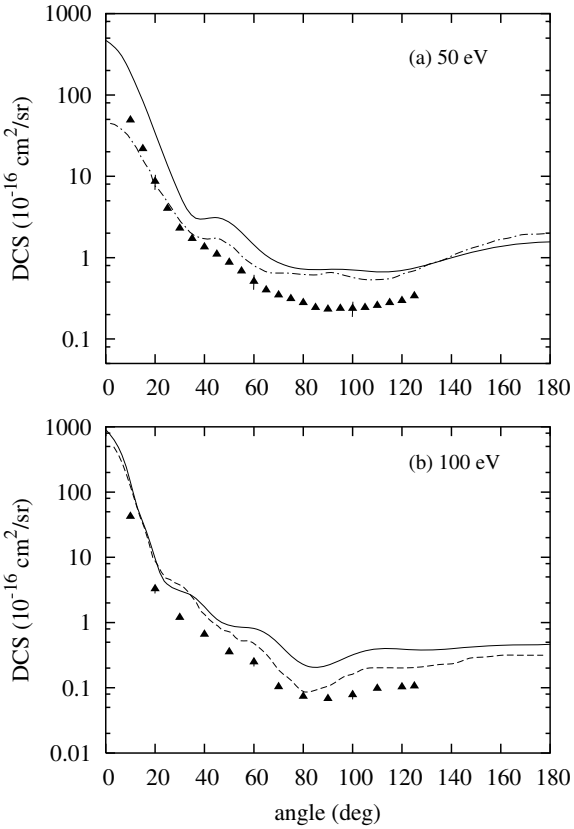

Figure 2. DCS for elastic e^-–C_4H_{10} collisions at (a) 50 eV and (b) 100 eV. Full triangles present experimental results; solid line presents calculated data using the IAM at the SEP level of approximation; dashed-dotted line, theoretical results of Lopes *et al* [12] using the Schwinger multichannel method; dashed-line, calculated data of Ma *et al* [27] using the IAM at the SEPA level of approximation. The intermediate scale marks in the *Y*-axis are respectively 2, 5 and 8 times the numbers appearing in the *Y*-scale for each decade.

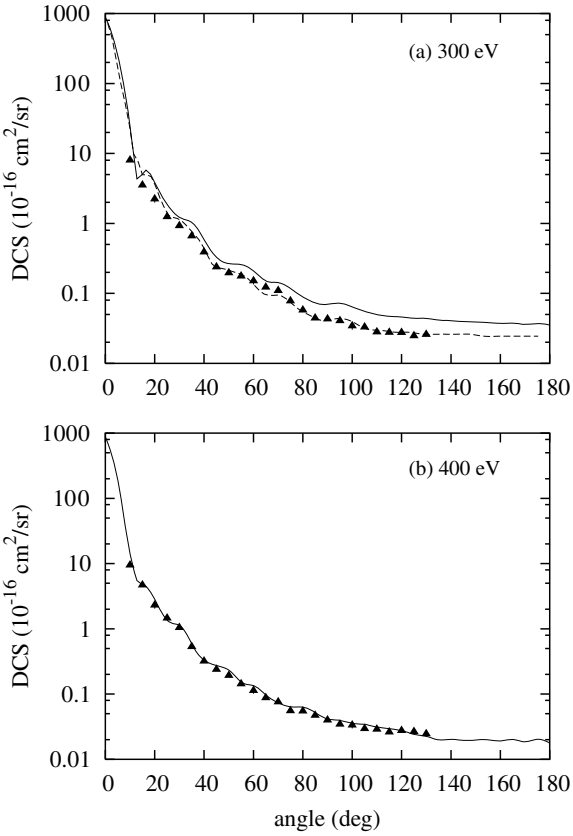

Figure 3. Same as in figure 2, but for (a) 300 eV and (b) 400 eV. The symbols used are the same as in figure 2.

The organization of this paper is as follows: in section 2, some experimental details are briefly presented. In section 3 we outline the calculation procedures. Finally, in section 4, our experimental results are compared with the present calculated results and with the existing theoretical and/or experimental data.

2. Experimental details

Details of our experimental setup and procedure have already been presented in our previous works [37, 38] and will only be briefly outlined here. A crossed electron beam–molecular beam geometry is used to measure the relative angular distribution of the scattered electrons at a given incident electron energy. The incident electron beam is produced by an electrostatically collimated gun with an estimated beam diameter of 1 mm. The scattered electrons are energy filtered by a retarding-field energy selector with a resolution of about 1.5 eV. With this resolution, it is sufficient to distinguish inelastically scattered electrons resulted from electronic excitation for the molecule under study since the excitation thresholds of benzene and *n*-butane are 4.97 eV and 7.4 eV [39], respectively. Nevertheless, it is unable to separate those from vibrational excitation processes. Therefore, our measured DCS are indeed vibrationally summed. During the measurements, the working pressure in the vacuum chamber is around 7×10^{-7} Torr. Benzene vapour was introduced into the vacuum chamber through a gas handling system connected to a glass balloon containing a liquid sample. The liquid benzene underwent a pre-treatment for degassing through several freeze–pump–thaw cycles. During this step a quadrupole mass spectrometer (Balzers Prisma QMS200) is used to verify the purity of the sample that is being introduced in the chamber. During the measurements, liquid benzene was maintained at the temperature of 0° C. At this temperature benzene vapour pressure is 30.8 Torr.

The recorded scattering intensities were converted into absolute elastic DCS using the RFT [34–36] . Accordingly, the DCS for the target under determination (x) can be related to known DCS of a secondary standard (std) as

$$(\mathrm{DCS})_x = (\mathrm{DCS})_{\mathrm{std}} \frac{I_x}{I_{\mathrm{std}}} \frac{n_{\mathrm{std}}}{n_x} \left(\frac{M_{\mathrm{std}}}{M_x} \right)^{\frac{1}{2}}, \qquad (1)$$

where I is the scattered electron intensity, n is the flow rate and M is the molecular weight. The above equation is valid if the beam profiles (density distribution) of both gases, x and std, are closely the same. According to Olander and Kruger [40], this requirement is fulfilled under two conditions: the equal mean-free paths (λ) of the gases behind the capillaries and the Knudsen number K_L defined as $\frac{\lambda}{L}$ varying between $\gamma \leqslant$

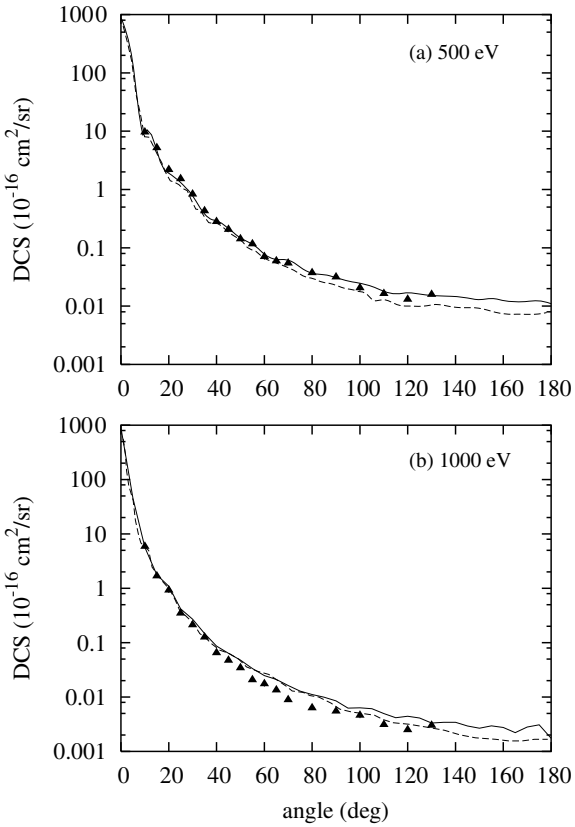

Figure 4. Same as in figure 2, but for (a) 500 eV and (b) 1000 eV. The symbols used are the same as in figure 2.

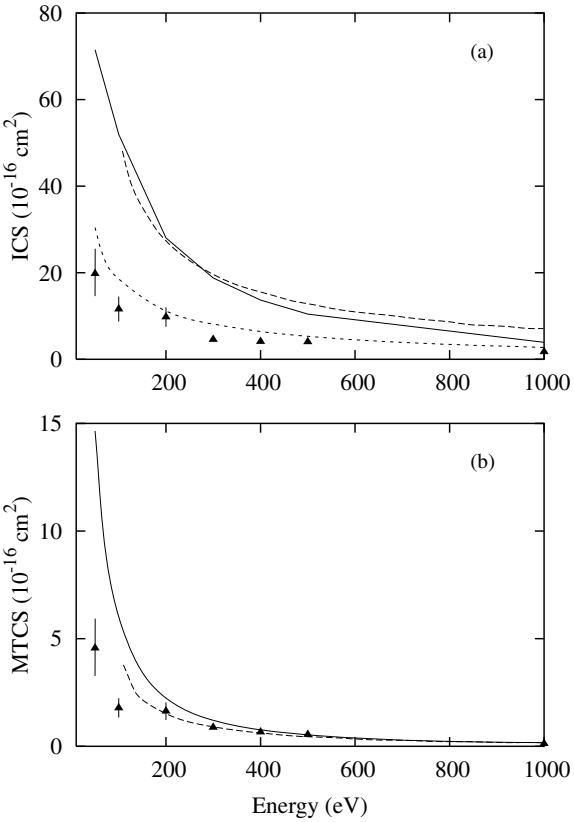

Figure 5. (a) ICS and (b) MTCS for elastic e^-–C_4H_{10} collisions. Full triangles present experimental results; solid line presents calculated data using the IAM at the SEP level of approximation; dashed-line, calculated data of Ma *et al* [27] using the IAM at the SEPA level of approximation; short-dashed line present calculated data using the AR.

$K_L \leqslant 10$, where $\gamma = d/L$ is the aspect ratio of the individual capillary with diameter d and length L. However, several recent investigations have provided experimental evidences that even at beam flow regimes in which the K_L's are significantly lower than γ, the above relationship can still be valid [36, 37]. In our apparatus, the gas inlet is formed by a single molybdenum tube with 1 mm diameter and 50 mm length, aspect ratio $\gamma = 0.02$. The estimated diameter of the produced gaseous beam is approximately 1 mm at the full-width at half-maximum (FWHM). In order to maintain the equal Knudsen number for different gases, we have considered hard-sphere diameters of 3.14 Å, 3.76 Å and 4.06 Å respectively for N_2, C_4H_{10} and C_6H_6 to set the pressures in the gas reservoir. These diameters were calculated from the respective van der Waals parameters [41].

In principle, any gaseous targets could be chosen as secondary standard. The only requirement is that reliable DCS covering the energy and angular ranges of interest are available in the literature for elastic electron scattering from the chosen target. In practice, the existence of a highly reliable DCS set for elastic e^-–He scattering in the low-energy range [42] makes this gas widely used as a secondary standard in the experimental DCS determinations. In 1993, Buckman *et al* [43] investigated the spatial profiles of effusive molecular beams for several gases. They found that the FWHM of the beam profiles were very similar for species Ar, Ne, N_2 and Kr in a wide range of λ (from 0.005 mm to 5 mm). On the other hand, the FWHM of He and H_2 beams are significantly smaller than those of heavier species at $\lambda \leqslant 0.1$ mm region. Based on the above observation, it can then be expected that the use of a secondary standard heavier than He would allow us to obtain accurate DCS for most of species, in a more extensive region of λ.

In the present study, N_2 [44, 45] is used as the secondary standard. Specifically, absolute DCS of Jansen *et al* [44] in the (200–1000) eV energy range and those of Dubois and Rudd [45] at 50 eV and 100 eV are used to normalize our data. Details of the analysis of experimental uncertainties have also been given elsewhere [37]. They are estimated briefly as follows. Uncertainties of a random nature such as pressure fluctuations, electron beam current readings, background scattering, etc, are estimated to be less than 2%. These contributions combined with the statistical uncertainties, estimated approximately as $N^{-\frac{1}{2}}$ of counting rates, give an overall uncertainty of 4% in the relative DCS for each gas. Also, the experimental uncertainty associated with the normalization procedure is estimated to be 7.5%. These errors were combined with the quoted errors of 6.6% [44], and 19% and 12%, respectively for 50 eV and 100 eV incident energies [45] in the absolute DCS of the secondary standard that leads to overall experimental uncertainties of 11% in our absolute DCS in the (200–1000) eV range, 21% at 50 eV and 15% at 100 eV. The absolute DCS were measured in the 10°–130°

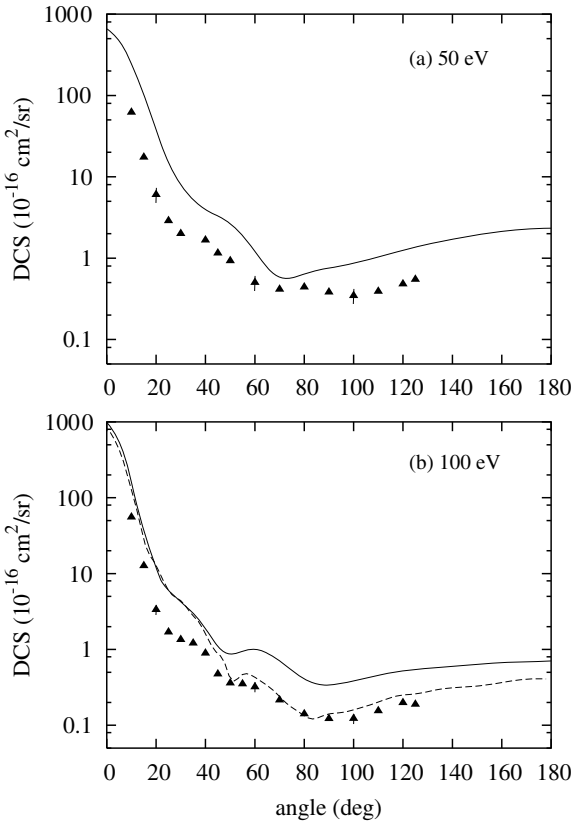

Figure 6. DCS for elastic e^-–C_6H_6 collisions at (a) 50 eV and (b) 100 eV. Full triangles present experimental results; solid line present calculated data using the IAM at the SEP level of approximation; dashed-line, calculated data of Ma *et al* [27] using the IAM at the SEPA level of approximation. The intermediate scale marks in the *Y*-axis are respectively 2, 5 and 8 times the numbers appearing in the *Y*-scale for each decade.

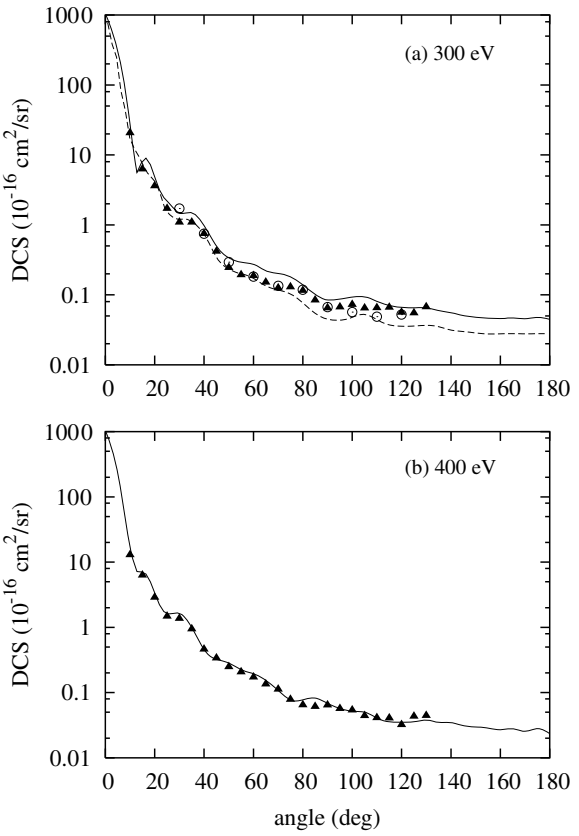

Figure 7. Same as in figure 6, but for (a) 300 eV and (b) 400 eV. The symbols used are the same as in figure 6, except: open circles, relative DCS of Mahant Shetty *et al* [25], normalized to our data at 40°.

angular range. In order to obtain ICS and MTCS, an extrapolation procedure was adopted to estimate DCS at scattering angles out of that range. The extrapolation was carried out manually. The overall errors on ICS and MTCS are estimated to be 23% in the (200–1000) eV range, 29% and 25% at 50 eV and 100 eV, respectively.

3. Calculation

In the IAM approach, the DCS for elastic electron scattering on a molecule, after averaging the molecular orientation in the space, is given as

$$\frac{\mathrm{d}\sigma}{\mathrm{d}\Omega} = \sum_{i}^{N}\sum_{j}^{N} f_i(\theta,k) f_j^*(\theta,k) \frac{\sin(sr_{ij})}{sr_{ij}}, \qquad (2)$$

where N is the number of atoms within a molecule, θ is the scattering angle and $f_i(\theta,k)$ is the complex scattering amplitude due to the ith atom in a molecule. In equation (2), $s = 2k\sin\left(\frac{\theta}{2}\right)$ is the magnitude of the transferred momentum during the collision and k is the magnitude of the linear momentum of the incident electron.

Atomic scattering amplitudes are obtained by solving the partial-wave radial Schrödinger equation

$$\left(\frac{\mathrm{d}^2}{\mathrm{d}r^2} - \frac{l(l+1)}{r^2} - 2\,V_{\mathrm{SEP}} + k^2\right) u_l(r) = 0, \qquad (3)$$

where V_{SEP} is the static-exchange-polarization potential, given as

$$V_{\mathrm{SEP}} = V_{\mathrm{stat}} + V_{\mathrm{ex}} + V_{\mathrm{pol}}. \qquad (4)$$

For carbon, the static (V_{stat}) and exchange (V_{ex}) contributions are derived from the near Hartree–Fock ground-state wavefunction, whereas for hydrogen, they are derived from the exact ground-state wavefunction. A parameter-free model potential introduced by Padial and Norcross [46] is used to account for the correlation–polarization contributions. In this model, a short-range correlation potential between the scattering and the target electrons is defined in an inner interaction region and a long-range polarization potential in an outer region. The correlation potential is calculated by a free-electron-gas model, derived using the target electronic density according to equation (9) of Padial and Norcross [46]. In addition, an asymptotic form of the polarization potential is used for the long-range electron–target interaction. The atomic polarizabilities as well as the internuclear distances used in the calculation are taken from the literature [41].

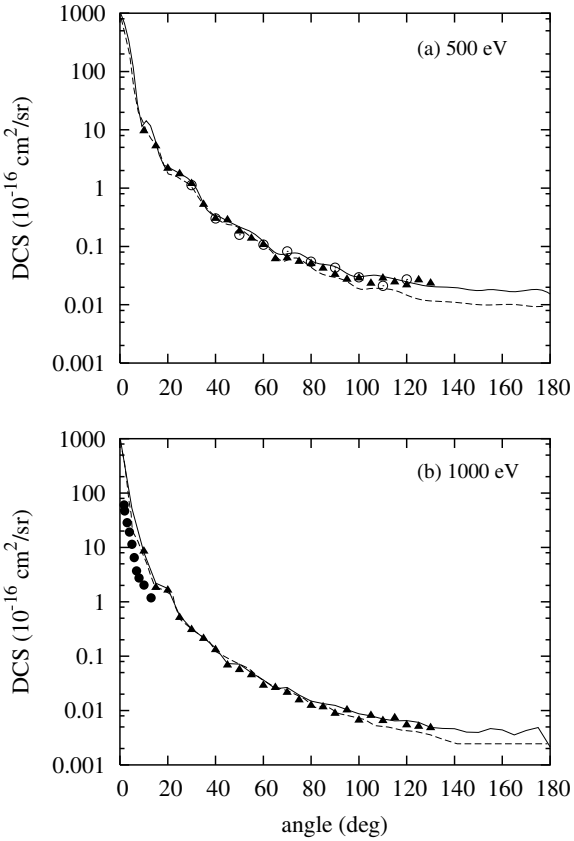

Figure 8. Same as in figure 7, but for (a) 500 eV and (b) 1000 eV. The symbols used are the same as in figure 7, except: full circles, experimental DCS of Boechat-Roberty *et al* [24].

Table 1. Acronyms used in this work.

DCS	Differential elastic cross sections
ICS	Integral cross sections
MTCS	Momentum-transfer cross sections
PICS	Partial ionization cross sections
TICS	Total ionization cross sections
TCS	Grand-total cross sections
IAM	Independent-atom model
SE	Static exchange
SEP	Static-exchange-polarization
SEPA	Static-exchange-polarization-absorption
SMC	Schwinger multichannel
AR	Additivity rule
SCAR	Screening-corrected additivity rule
RFT	Relative-flow technique
FWHM	Full-width at half-maximum

The ICS ($\sigma_I(E)$) and the MTCS ($\sigma_M(E)$) for elastic electron–molecule scattering are defined as

$$\sigma_I(E) = 2\pi \int_0^{\pi} \frac{d\sigma}{d\Omega} \sin\theta \, d\theta \tag{5}$$

and

$$\sigma_M(E) = 2\pi \int_0^{\pi} \frac{d\sigma}{d\Omega} (1 - cos(\theta)) \sin\theta \, d\theta, \tag{6}$$

respectively, where E is the incident energy.

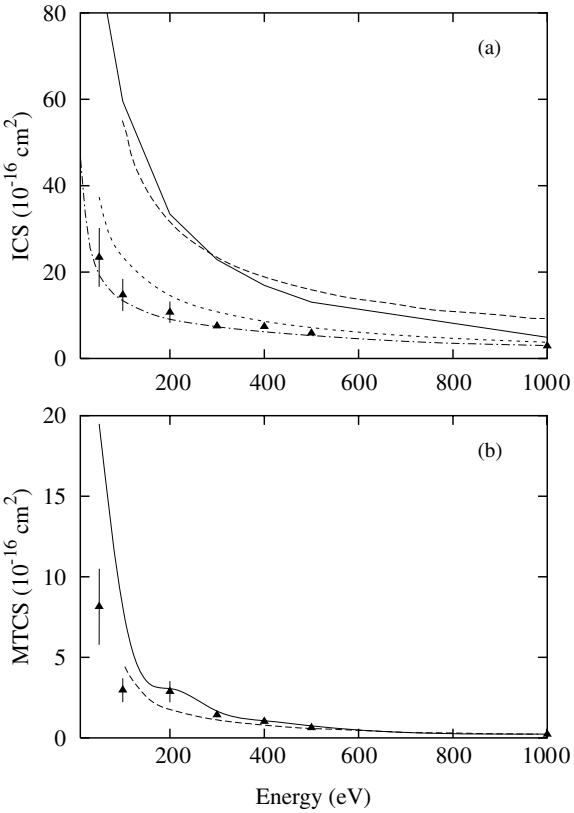

Figure 9. (a) ICS and (b) MTCS for elastic e^-–C_6H_6 collisions. Full triangles present experimental results; solid line presents calculated data using the IAM at the SEP level of approximation; dashed-line, calculated data of Ma *et al* [27] using the IAM at the SEPA level of approximation; short-dashed line present calculated data using the AR; dashed-dotted line, the calculated results of Blanco and García [31] using the SCAR.

4. Results and discussion

The present experimental data of DCS, ICS and MTCS, obtained in the (50–1000) eV energy range, are presented in tables 2 and 3 for *n*-butane and benzene, respectively. Some representative results of DCS at selected incident energies are also plotted. In figures 2–4, we present our experimental DCS for electron scattering by *n*-butane in the (50–1000) eV incident energy range. There, the theoretical results of Lopes *et al* [12] at 50 eV, the present IAM results at the SEP level of approximation as well as the calculated results of Ma *et al* [27] using the improved version of IAM at the SEPA level are also shown for comparison. In their study, Ma *et al* [27] included a model absorption potential to represent the effects of inelastic scattering channels on elastic collisions. At 50 eV, the calculated results of Lopes *et al* using the SMC at the SE level reproduce quite well the shape of the measured data. Quantitatively, the theoretical DCS agreement is about 17% above our measured data at scattering angles up to 40°. Nevertheless at larger angles, their calculation significantly overestimates (about a factor of 2) the experimental DCS possibly due to the neglect of absorption effects. At 50 eV and 100 eV, the present IAM calculations also provide good description of the shape of the

Table 2. Experimental DCS, ICS and MTCS[a] for elastic e^-–C_4H_{10} scattering.

Angle (°)	E_0 (eV)						
	50	100	200	300	400	500	1000
10	4.91(1)[b]	4.22(1)	3.56(1)	8.00(0)	9.47(0)	9.64(0)	5.86(0)
15	2.18(1)		6.43(0)	3.51(0)	4.68(0)	5.17(0)	1.68(0)
20	8.63(0)	3.28(0)	2.83(0)	2.22(0)	2.29(0)	2.18(0)	9.26(−1)
25	4.02(0)		2.11(0)	1.24(0)	1.45(0)	1.52(0)	3.48(−1)
30	2.30(0)	1.19(0)	1.23(0)	9.23(−1)	1.04(0)	8.29(−1)	2.10(−1)
35	1.71(0)		8.10(−1)	6.60(−1)	5.31(−1)	4.29(−1)	1.26(−1)
40	1.35(0)	6.57(−1)	6.55(−1)	3.90(−1)	3.20(−1)	2.81(−1)	6.49(−2)
45	1.10(0)		5.10(−1)	2.40(−1)	2.40(−1)	2.05(−1)	4.69(−2)
50	8.73(−1)	3.54(−1)	3.02(−1)	1.96(−1)	1.90(−1)	1.42(−1)	3.39(−2)
55	6.82(−1)		1.86(−1)	1.76(−1)	1.43(−1)	1.16(−1)	1.98(−2)
60	5.10(−1)	2.49(−1)	1.39(−1)	1.50(−1)	1.13(−1)	7.02(−2)	1.75(−2)
65	4.00(−1)		1.45(−1)	1.22(−1)	8.74(−2)	5.93(−2)	1.34(−2)
70	3.46(−1)	1.03(−1)	1.34(−1)	1.10(−1)	7.60(−2)	5.43(−2)	8.90(−3)
75	3.12(−1)		1.20(−1)	7.80(−2)	5.50(−2)		
80	2.79(−1)	7.36(−2)	1.00(−1)	5.70(−2)	5.46(−2)	3.72(−2)	6.20(−3)
85	2.43(−1)		8.70(−2)	4.43(−2)	4.70(−2)		
90	2.32(−1)	6.82(−2)	9.00(−2)	4.30(−2)	4.00(−2)	3.15(−2)	5.50(−3)
95	2.37(−1)		8.50(−2)	4.10(−2)	3.40(−2)		
100	2.37(−1)	7.81(−2)	7.20(−2)	3.40(−2)	3.34(−2)	2.05(−2)	4.60(−3)
105	2.43(−1)		6.80(−2)	3.30(−2)	2.90(−2)		
110	2.58(−1)	9.75(−2)	7.10(−2)	2.80(−2)	2.90(−2)	1.64(−2)	3.10(−3)
115	2.79(−1)		7.04(−2)	2.80(−2)	2.61(−2)		
120	2.96(−1)	1.03(−1)	7.80(−2)	2.70(−2)	2.74(−2)	1.30(−2)	2.50(−3)
125	3.38(−1)	1.06(−1)	8.00(−2)	2.46(−2)	2.64(−2)		
130			8.60(−2)	2.50(−2)	2.45(−2)	1.58(−2)	3.00(−3)
ICS	1.98(1)	1.16(1)	9.76(0)	4.55(0)	4.10(0)	4.02(0)	1.72(0)
MTCS	4.60(0)	1.78(0)	1.63(0)	8.76(−1)	6.56(−1)	5.43(−1)	1.25(−1)

[a] DCS are given in 10^{-16} cm^2 sr^{-1}, ICS and MTCS in 10^{-16} cm^2.
[b] 4.91(1) means 4.91×10^1.

experimental data, but the calculated DCS overestimate the experimental values by nearly a factor of 3 for all scattering angles covered in this work. At 100 eV, the calculated results of Ma *et al* show a better agreement (a factor of 2 in average) with the experimental DCS at intermediate and large scattering angles due to the incorporation of absorption effects. Also, an extended structural factor which accounts partially for the overlapping effect of electronic clouds of adjacent atoms may also contribute to this better agreement. Moreover, the reliability of IAM-based calculations improves with increasing energy in the sense that at energies above 400 eV, the calculations at both the SEP and SEPA levels can provide DCS in marginal agreement (14%) with the experimental data.

In figures 5(a) and (b) we present our experimental ICS and MTCS, respectively, for elastic electron scattering by *n*-butane in the (50–1000) eV energy range in comparison with the present calculated data using the IAM at the SEP level and the IAM SEPA results of Ma *et al* [27]. In addition, the present calculated ICS using the AR are also shown for comparison. It is seen that the two sets of ICS calculated using the IAM lie systematically above the experimental data. Specifically at lower energies, the IAM-based theories overestimate the experimental values by a factor of about 3. Nevertheless, the discrepancies between theory and experiment reduce with increasing incident energies. At 1000 eV, the present IAM ICS lie approximately 80% above the experimental data. Although the ICS calculated using the AR are in significantly better agreement with the experimental data (40% above in the covered energy range) than their IAM counterparts, this could be merely fortuitous and is caused from some form of error compensations. Indeed, the AR ICS are obtained by summing up the electron scattering ICS of atomic constituent of the target. Therefore, terms arising from interferences of the atomic scattering amplitudes are neglected. At scattering angles near the forward direction, the contribution of such terms to DCS can be as large as 60%. On the other hand, it is interesting that the two sets of IAM ICS are quite similar to each other. This is due to the fact that the absorption effects act mainly in the intermediate and large scattering angles. The DCS at the small angles, which contribute dominantly to the ICS, are practically unaffected by the incorporation of such effects.

In figure 5(b) it is seen that in general, the MTCS calculated using both the IAM-based methods agree with the experimental data within the experimental uncertainties at energies above 200 eV. Nevertheless at energies up to 100 eV, IAM MTCS are approximately three times the experimental values.

In figures 6–8, we compare the experimental DCS for elastic electron scattering by benzene in the (50–1000) eV incident energy range with the experimental results of Boechat-Roberty *et al* [24] at 1000 eV and with the relative DCS of Mahant Shetty *et al* [25] at 300 eV and 500 eV, normalized to our absolute data at 40°. The present calculated data using the IAM at the SEP level of approximation in the

Table 3. Experimental DCS, ICS and MTCS[a] for elastic e^-–C_6H_6 scattering.

Angle (°)	E_0 (eV)						
	50	100	200	300	400	500	1000
10	6.19(1)[b]	5.55(1)	3.55(1)	2.07(1)	1.29(1)	9.55(0)	8.51(0)
15	1.74(1)	1.27(1)	7.33(0)	6.29(0)	6.20(0)	5.28(0)	2.04(0)
20	6.03(0)	3.34(0)	3.45(0)	3.60(0)	2.88(0)	2.17(0)	1.63(0)
25	2.88(0)	1.69(0)	2.69(0)	1.71(0)	1.48(0)	1.75(0)	5.12(−1)
30	1.99(0)	1.34(0)	1.47(0)	1.08(0)	1.36(0)	1.19(0)	3.11(−1)
35	1.93(0)	1.21(0)	9.60(−1)	1.09(0)	9.45(−1)	5.22(−1)	2.11(−1)
40	1.66(0)	8.90(−1)	9.00(−1)	7.51(−1)	4.61(−1)	3.01(−1)	1.31(−1)
45	1.15(0)	4.73(−1)	8.42(−1)	4.18(−1)	3.34(−1)	2.83(−1)	6.81(−2)
50	9.25(−1)	3.60(−1)	5.95(−1)	2.45(−1)	2.48(−1)	1.82(−1)	5.61(−2)
55		3.51(−1)	3.57(−1)	1.93(−1)	2.07(−1)	1.38(−1)	4.53(−2)
60	5.00(−1)	3.21(−1)	2.56(−1)	1.87(−1)	1.72(−1)	1.07(−1)	2.90(−2)
65			2.32(−1)	1.52(−1)	1.34(−1)	6.10(−2)	2.64(−2)
70	4.13(−1)	2.15(−1)	2.03(−1)	1.26(−1)	1.12(−1)	6.35(−2)	2.14(−2)
75			1.93(−1)	1.30(−1)	7.84(−2)	5.51(−2)	1.56(−2)
80	4.40(−1)	1.41(−1)	1.92(−1)	1.15(−1)	6.47(−2)	5.04(−2)	1.24(−2)
85			1.79(−1)	8.43(−2)	6.12(−2)	4.21(−2)	1.16(−2)
90	3.81(−1)	1.22(−1)	1.69(−1)	6.50(−2)	6.43(−2)	3.29(−2)	8.60(−3)
95			1.69(−1)	6.69(−2)	5.67(−2)	2.72(−2)	1.02(−2)
100	3.46(−1)	1.22(−1)	1.46(−1)	7.26(−2)	5.40(−2)	2.87(−2)	6.60(−3)
105			1.30(−1)	6.47(−2)	4.42(−2)	2.32(−2)	8.10(−3)
110	3.89(−1)	1.54(−1)	1.28(−1)	6.52(−2)	4.10(−2)	2.85(−2)	6.30(−3)
115			1.40(−1)	6.62(−2)	4.06(−2)	2.45(−2)	7.30(−3)
120	4.81(−1)	1.98(−1)	1.50(−1)	5.63(−2)	3.21(−2)	2.18(−2)	6.00(−3)
125	5.47(−1)	1.89(−1)	1.53(−1)	5.52(−2)	4.33(−2)	2.66(−2)	5.40(−3)
130			1.66(−1)	6.74(−2)	4.45(−2)	2.33(−2)	4.80(−3)
ICS	2.34(1)	1.47(1)	1.07(1)	7.49(0)	7.36(0)	5.86(0)	2.87(0)
MTCS	8.14(0)	2.96(0)	2.87(0)	1.42(0)	1.01(0)	6.27(−1)	2.15(−1)

[a] DCS are given in 10^{-16} cm^2 sr^{-1}, ICS and MTCS in 10^{-16} cm^2.
[b] 6.19(1) means 6.19×10^1.

energy range covered herein and the calculated data of Ma *et al* [27] also using the IAM but at SEPA level at 100 eV and above are also shown. At 50 eV and 100 eV, there is a qualitative agreement between the calculated DCS using the IAM and experimental data. Similar to that observed for *n*-butane, the calculations with incorporation of absorption effects are in better agreement with experiments in the intermediate and large angular ranges. For instance at 100 eV, the present IAM DCS is about 2.5 times the experimental data. For angles above 45°, the IAM with absorption of Ma *et al* [27] lie within the experimental uncertainties. Again, the agreement between the IAM DCS and experimental data improves significantly with increasing energy. At 300 eV and above, there is a general good agreement (about 25% of discrepancy). At 300 eV and 500 eV, the normalized DCS of Mahant Shetty *et al* [25] agree very well with our experimental data in the overlapped angular range. At 1000 eV, the absolute DCS of Boechat-Roberty *et al* are reported only at scattering angles up to 13°, therefore do not overlap with our data. However, their results is about one-fourth of the IAM data. In contrast, there is a very good agreement (within the estimated experimental uncertainties) between our measured DCS and the calculated data using the IAM-based formalisms.

In figures 9(a) and (b) we show our experimental ICS and MTCS, respectively, for elastic electron scattering by benzene in the (50–1000) eV energy range in comparison with the present calculated results using the IAM at the SEP level of approximation. The ICS calculated using the IAM at SEPA level of Ma *et al* [27], the present ICS using the AR, and the ICS of Blanco and García [31] using the screening-corrected additivity rule (SCAR) are also shown. As is seen for *n*-butane, the IAM-based calculations overestimate the ICS from a factor of 3.3 at 50 eV to a factor of 1.5 at 1000 eV. However, the agreement between the IAM MTCS and experimental results is very good (within the estimated experimental uncertainties) for energies above 200 eV, whereas at lower energies the largest discrepancy between theories and experiments is a factor of 2.5 at 50 eV. On the other hand, there is a generally good agreement between the experimental ICS and those calculated using the AR-based methods. In particular, the SCAR ICS lie within the experimental uncertainties in the covered energy range. This good agreement is possibly due to the error compensations as already mentioned above.

In figures 10(a) and (b) we present a comparison of the existing experimental data in the (10–1000) eV range for electron collisions with *n*-butane and benzene, respectively. For benzene, the TICS calculated using the BEB model [47] is also shown. For both targets, the contribution of the elastic ICS is about 50% of the TCS in the (50–200) eV range. As expected, the contribution of elastic scattering channel is dominant at very low incident energies. Above 200 eV, the contribution of elastic collisions varies around 30–40% of TCS. On the other hand, the magnitudes of elastic MTCS are much smaller than ICS in the (50–1000) eV. It is mainly due to the fact that the DCS in this energy range are in general forward peaked. The ionization process constitutes the most

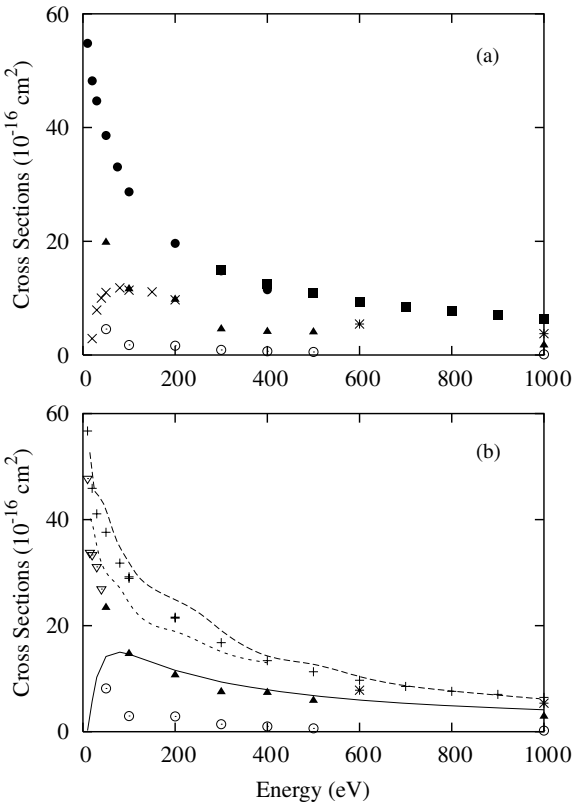

Figure 10. Comparison of the existing experimental results for electron scattering by (a) *n*-butane (b) benzene in the (10–1000) eV range. In (a), full triangles present results for ICS; open circles present results for MTCS; solid circles, experimental TCS of Floeder *et al* [15]; full squares, experimental TCS of Ariyasinghe *et al* [14]; crosses, experimental TICS of Jiao *et al* [5]; asterisks: experimental TICS of Schram *et al* [16]. In (b), full triangles present results for ICS; open circles present results for MTCS; open triangle, experimental ICS of Cho *et al* [23]; dashed line, experimental TCS of Makochekanwa *et al* [17]; short-dashed line, experimental TCS of Sueoka [18]; pluses, experimental TCS of Mozejko *et al* [19]; asterisks: experimental TICS of Schram *et al* [16]; solid line, calculated TICS using the BEB of Hwang *et al* [47].

important contribution of the inelastic collisions for energies above 100 eV. The experimental TICS reported by Schram *et al* show contributions higher than 50% of the TCS for incident energies above 600 eV. Specifically for benzene the contribution of ionization channel represents up to 65% of TCS at 1000 eV.

In summary, the present study reports experimental DCS, ICS and MTCS for elastic electron scattering by *n*-butane and benzene. Some of these results are reported by the first time. The comparison of our results with the present and existing theoretical data shows significant discrepancies, particularly at incident energies below 200 eV. At higher energies, the IAM-based calculations can in general provide quite reliable DCS for scattering angles larger than 15°. Nevertheless, even at energies as high as 1000 eV, the IAM-based calculations still overestimate significantly the ICS. Such a discrepancy is mainly due to the overestimation of the IAM DCS at angles near the forward direction. On the other hand, despite the neglect of the interference terms in the scattering amplitudes, the AR-based calculations can provide ICS in better agreement with experimental data, which is interesting. Nevertheless, the general use of AR-based calculations to estimate electron–molecule scattering ICS still require more tests, particularly for targets containing other atomic constituent than C and H. For that purpose, more experimental cross sections are needed and some of such measurements for small alcohols are now in progress.

Acknowledgments

This research was partially supported by the Brazilian agencies CNPq and FAPESP.

References

[1] Janev R K and Reiter D 1004 *Phys. Plasmas* **11** 708
[2] Janev R K 1993 *Atomic and Plasma-Material Interaction Processes in Controlled Thermonuclear Fusion* ed R K Janev and H W Drawin (Amsterdam: Elsevier) p 27
[3] Kim Y, Ferreti V W, Rosocha L A, Anderson G K, Abbate S and Kim K-T 2006 *IEEE Trans. Plasma Sci.* **34** 2532
[4] Liu J, Li G, Kuthi A, Gutmark E J, Ronney P D and Gundersen M A 2005 *IEEE Trans. Plasma Sci.* **33** 326
[5] Jiao C Q, DeJoseph C A Jr and Garscadden A 2007 *J. Phys. D: Appl. Phys.* **40** 409
[6] Wilson E H, Atreya S K and Coustenis A 2003 *J. Geophys. Res.* **108** 5014
[7] Cernicharo J, Heras A M, Tielas A G G M, Pardo J R, Herpin F, Guélin M and Waters L B F M 1997 *Astrophys. J.* **546** L123
[8] Winstead C, McKoy V and Sanchez S D 2007 *J. Chem. Phys.* **127** 085105
[9] Baccarelli I, Gianturco F A, Grandi A, Sanna N, Lucchese R R, Bald I, Kopyra J and Illenberger E 2007 *J. Am. Chem. Soc.* **129** 6269
[10] Gianturco F A and Lucchese R R 1998 *J. Chem. Phys.* **108** 6144
[11] Bettega M H F, Winstead C and McKoy V 2000 *J. Chem. Phys.* **112** 8806
[12] Lopes A R, Bettega M H F, Lima M A P and Ferreira L G 2004 *J. Phys. B: At. Mol. Opt. Phys.* **37** 997
[13] Karwasz G P, Brusa R S and Zecca A 2001 *Riv. Nuovo Cimento* **24** 1
[14] Ariyasinghe A, Wickramarachchi P and Palihawadana P 2007 *Nucl. Instrum. Methods Phys. Res.* B **259** 841
[15] Floeder K, Fromme D, Raith W, Schwab A and Sinapius G 1985 *J. Phys. B: At. Mol. Phys.* **18** 3374
[16] Schram B L, van der Wiel M J, de Heer F J and Moustafa H R 1966 *J. Chem. Phys.* **44** 49
[17] Makochekanwa C, Sueoka O and Kimura M 2003 *Phys. Rev.* A **68** 032707
[18] Sueoka O 1988 *J. Phys. B: At. Mol. Opt. Phys.* **21** L631
[19] Mozejko P, Kasperski G, Szmytkowski C, Karwasz G P, Brusa R S and Zecca A 1996 *Chem. Phys. Lett.* **257** 309
[20] Gulley R J, Lunt S L, Ziesel J-P and Field D 1998 *J. Phys. B: At. Mol. Opt. Phys.* **31** 2735
[21] Beenakker C I M and de Heer F J 1974 *Chem. Phys. Lett.* **29** 89
[22] Gulley R J and Buckman S J 1999 *J. Phys. B: At. Mol. Opt. Phys.* **32** L405
[23] Cho H, Gulley R J, Sunohara K, Kitajima M, Uhlmann L J, Tanaka H and Buckman S J 2001 *J. Phys. B: At. Mol. Opt. Phys.* **34** 1019
[24] Boechat-Roberty H M, Rocco M L M, Lucas C A and de Souza G G B 2004 *J. Phys. B: At. Mol. Opt. Phys.* **37** 1467

[25] Mahant Shetty J S, Bharathi S M and Basavaraju G 1992 *Pramana J. Phys.* **39** 297
[26] Bettega M H F, Lima M A P and Ferreira L G 2007 *J. Phys. B: At. Mol. Opt. Phys.* **40** 3015
[27] Ma E J, Ma Y G, Cai X Z, Fang D-Q, Shen W-Q and Tian W-D 2008 *Chin. Phys. Lett.* **25** 97
[28] Shi D, Sun J, Zhu Z, Liu Y and Yang X 2006 *Chin. Phys.* **15** 1278
[29] Shi D, Sun J, Liu Y and Zhu Z 2008 *J. Phys. B: At. Mol. Opt. Phys.* **41** 025205
[30] Blanco F and García G 2003 *Phys. Lett.* A **317** 458
[31] Blanco F and García G 2007 *Phys. Lett.* A **360** 707
[32] Lee M T, Iga I, Machado L E, Brescansin L M, Castro E A Y, Sanches I P and de Souza G L C 2007 *J. Electron Spectrosc. Relat. Phenom.* **155** 14
[33] Castro E A Y, de Souza G L C, Iga I, Machado L E, Brescansin L M and Lee M T T 2007 *J. Electron Spectrosc. Relat. Phenom.* **159** 30
[34] Srivastava S K, Chutjian A and Trajmar S 1975 *J. Chem. Phys.* **63** 2659
[35] Khakoo M A and Trajmar S 1986 *Phys. Rev.* A **34** 138
[36] Tanaka H, Ishikawa T, Masai T, Sagara T, Boesten L, Takekawa M, Itikawa Y and Kimura M 1998 *Phys. Rev.* A **57** 1798
[37] Iga I, Lee M T, P. Homem M G, Machado L E and Brescansin L M 2000 *Phys. Rev.* A **61** 227081
[38] Rawat P, Iga I, Lee M T, Brescansin L M, Machado L E and Homem M G P 2003 *Phys. Rev.* A **68** 052711
[39] Robin M B 1974 *Higher Excited States of Polyatomic Molecules* (New York: Academic)
[40] Olander D R and Kruger V 1970 *J. Appl. Phys.* **41** 2769
[41] Lide D R 1992–1993 *Handbook of Chemistry and Physics* 73rd edn ed David R Lide (Boca Raton, FL: CRC Press)
[42] Register D F, Trajmar S and Srivastava S K 1980 *Phys. Rev.* A **21** 1134
[43] Buckman S J, Gulley R J, Moghbelalhossein M and Bennett S J 1993 *Meas. Sci. Technol.* **4** 1143
[44] Jansen R H J, de Heer F J, Luyken H J, van Wingerden B and Blaauw M E 1976 *J. Phys. B: At. Mol. Phys.* **9** 185
[45] DuBois R D and Rudd M E 1976 *J. Phys. B: At. Mol. Phys.* **9** 2657
[46] Padial N Y and Norcross D W 1984 *Phys. Rev.* A **29** 1742
[47] Hwang W, Kim W-K and Rudd M E 1996 *J. Chem. Phys.* **104** 2956